ELSEVIER

Cement and Concrete Composites **20** (1998) 13–29

Printed in Great Britain
0958-9465/98/$19.00

PII:S0958-9465(97)00073-50

Ferrocement Bolted Shear Joints: Failure Modes and Strength Prediction

H. Hammoud,* & A. E. Naaman

The University of Michigan, Dept. of Civil & Environmental Engrg, 2340 G. G. Brown Bldg, Ann Arbor, MI 48109-2125, USA

(Received 30 September 1997; accepted 24 November 1997)

Abstract

*An experimental investigation was carried out to study the behavior of ferrocement bolted shear joints. Twenty-eight different pin-loaded ferrocement plate configurations and eight control specimens were tested. The test variables were the type of mesh (square, hexagonal, mixed), mesh orientation (0/90° or ±45°), number of mesh layers (2 to 8 corresponding to a volume fraction from 1.68% to 6.72%), and ratio between end distance and hole diameter (*e/d = 4 *or 6). Three failure modes were observed, net tensile section failure, cleavage failure, and crushing compression failure at the bolt. Cleavage failure was predominant for* e/d = 4*, and net-section tension failure or compression crushing for* e/d = 6*. The strength of the mesh reinforcement was closely related to the strength of the specimens that failed in the cleavage and net-section modes. Prediction equations are developed based on the Limit analysis Lower Bound Theorem to predict the net tension or cleavage failure loads, and a conservative equation is proposed to predict compression crushing failure. A comparison was made with other prediction equations available in the literature.*

Keywords: bolted connections, bearing joints, moment joints, ferrocement connections, tensile strength, cement composites, bolts, connections, joints, panels, pin-loaded plates.

*Correspondence to: Dr H. Hammoud.

INTRODUCTION

Applications where bolted ferrocement joints can be used range from water tanks, irrigation channels, and roof panels to entirely panelized housing systems where the connections between panels are bolted. Most of the research work on bolted connections available in the literature is on steel and on resin-based composite materials. Comprehensive reviews on the mechanics of bolted connections, and the behavior of bolted connections in steel and resin-based composites ar available in the literature.[1–5] Only one published study[6] was found on ferrocement bolted connections at the time of this study.[7]

A panelized ferrocement housing system using bolted joints has been described in two previous publications,[8,9] and the bolted connections were shown to transfer a combination of axial force, moment and shear force between the ferrocement panels. This combination ultimately causes shear and axial forces to be transferred by the bolts. Therefore, bolted joints were divided in two fundamental types, shear joints and moment joints (also often called axial joints). A study on moment resisting joints has previously been presented.[10] This study focuses on the behavior of shear joints. The results of an experimental investigation and simplified strength predictions equations are presented. The experimental results and the prediction equations are compared with those given by Mansur *et al.*[11] A number of practical conclu-

sions are drawn. Although an extensive finite element analysis was carried out to complement the experimental investigation, its results are left for another publication.[12]

RESEARCH SIGNIFICANCE

Bolted connections are essential in prefabrication. This is the case for ferrocement structural systems, particularly housing systems, where panels are used. To ensure the economic and safe use of ferrocement bolted joints, a clear understanding of their mechanical behavior is needed. This understanding can be best achieved at present by a combination of an experimental program and analytical (here a finite element analysis) program to identify the failure modes, strengths, and stress distribution. Based on the results of such an approach, simple strength prediction equations could be developed for design.

EXPERIMENTAL PROGRAM

A total of 28 different pin-loaded ferrocement plate configurations and eight control specimens were tested under direct tension. The parameters studied during the experimental investigation are (Fig. 1):

(1) Ratio e/d is the ratio between the end distance e (distance between the center of the bolt and the plate edge) to the hole diameter d. The two ratios investigated were $e/d = 4$ and $e/d = 6$, corresponding to end distances of 2.0″ (50.8 mm) and 3.0″ (76.2 mm) (the hole diameter was kept constant at $d = 0.5$″ (12.7 mm)).
(2) Type of mesh: welded square mesh ($1/4 \times 1/4$ wire spacing) and hexagonal mesh (3/4″ (19.05 mm) opening) were used.
(3) Mesh orientation: the square mesh was utilized in two different orientations relative to the plate, parallel to the sides of the plate (0/90°) and at $\pm 45°$ degrees angle. These two configurations will also be called 'square' and 'inclined' in this study. In the configuration called 'hexagonal', the specimens were reinforced with the hexagonal mesh keeping the longitudinal mesh direction (direction of

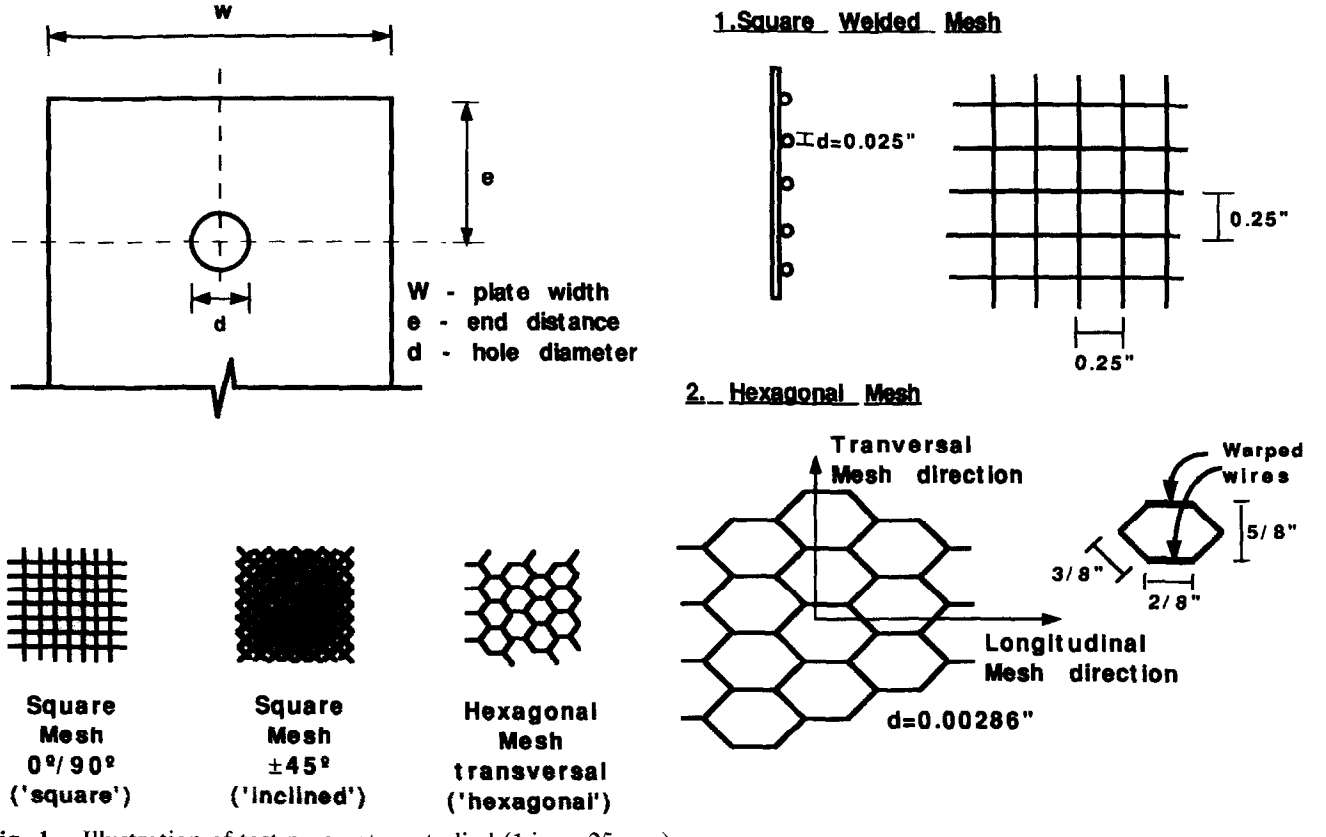

Fig. 1. Illustration of test parameters studied (1 in. = 25 mm)

warped wires) perpendicular to the load direction.

(4) Number of mesh layers (volume fraction of reinforcement): for every type and orientation of mesh, specimens reinforced with 2, 4, 6 and 8 layers were tested. This corresponds to volume fractions of 1.68, 3.36, 5.04 and 6.7% for the square mesh, and 0.96, 1.92, 2.88 and 3.84% for the hexagonal mesh. Furthermore, four specimens were reinforced with a combination of different types of mesh; they are called 'mixed'; they are reinforced with four layers of square mesh and additional layers of either the hexagonal or the inclined mesh.

The cement mortar was fabricated with ASTM Type III high early strength cement. The fine aggregate used was a graded silica Ottawa sand, ASTM C-109. The mix proportions in weight were cement = 1.0, sand = 2.0, water = 0.4, superplasticizer (Melment) = 0.025. The mortar mechanical properties were obtained by testing 3×6 cylinders. The average compressive strength attained for the specimens was 8.5 ksi (58.6 MPa) at 15 days. As for the reinforcement, two types of mesh were utilized, namely a square-welded mesh and an hexagonal mesh. The square mesh used had a 0.25-in. (6.35 mm) spacing between wires, the wires had an average diameter of 0.025 in. (0.635 mm), and the volume of mesh per unit area was 0.0042 $in.^3/in.^2$ (0.1067 mm^3/mm^2). The hexagonal mesh used had a wire diameter of 0.00286 in. (0.0726 mm), and a volume of mesh per unit area of 0..0024 $in.^3/in.^2$ (0.061 mm^3/mm^2). The bolts utilized to load the plates were standard grade 2 Hex Cap Screws with a 0.5 in. (12.7 mm) diameter and 2.5 in. (63.5 mm) length (Grade 2, 1/2 in., 2.5 in.). Both the bolt's shank and threaded portions had a length of 1.25 in. (31.75 mm)

The pin-loaded specimens were rectangular ferrocement plates 12 in. (304.8 mm) long, 5 in. (127.0 mm) wide and 0.5 in. (12.7 mm) thick ($12'' \times 5'' \times 0.5''$), and the control specimens were 12 in. (304.8 mm) long, 3 in. (76.2 mm) wide and 0.5 in. (127.0 mm) thick ($12'' \times 3'' \times 0.5''$). The reinforcing mesh was cut into the proper dimensions, and slotted at the position of the specimens' holes, if present. Plexiglas molds were used, and steel pins were glued to the internal walls of the molds in the locations of holes. The reinforcing mesh was then carefully placed inside the mold to fit the glued pins in the position of the holes. The internal surface of the mold and the pin's external surface were coated with oil to facilitate specimen and pin removal.

The mortar was mixed in a small food type mixer. The cement and sand were properly mixed first, and then water and superplasticizer were added to the solution. The molds were then placed into a vibrating table and the mortar was poured. The specimens were removed from the forms 24 hours after pouring. At this point, the steel pins (if present) were removed from the specimens, and the specimens were placed in a water tank where they cured for about 15 days. Then, they were left in laboratory environment until tested. All specimens were finally coated with a lime solution for better observation of cracks during testing.

Control specimens had no bolts and were tested in direct tension. Prior to testing, aluminum plates were glued to both sides of the plates along a 2-in. (50.8 mm) length at the end portions, to minimize failure at the gripping of the machine jaws. This was done with a fast-curing Epoxy adhesive.

Test set-up and instrumentation

The ferrocement rectangular plates were pin-loaded in tension by two bolts inserted in the holes (Fig. 2). One of the bolts was fixed to the machine table while the other, the driving bolt, was attached to the cross-head of the testing machine and transferred the load to the specimen. This set-up was meant to reproduce the behavior of the plates in a real shear-type connection. The specimens were tested in an INSTRON machine with 30 kips (133.4 kN) capacity in tension and compression. The specimens were tested under displacement control with a rate of loading of 0.01 inch/min (0.254 mm/min). All measurements were collected by a data acquisition system controlled by a PC computer, and the values of the applied loads and displacements were recorded (Fig. 3). An optical motion measuring instrument (Optotrack) was used in addition to the machine load cell and linear voltage differential transducers (LVDTs) as described next. Optotrack can track the tri-dimentional coordinates of infrared markers glued to the specimen at desired locations.

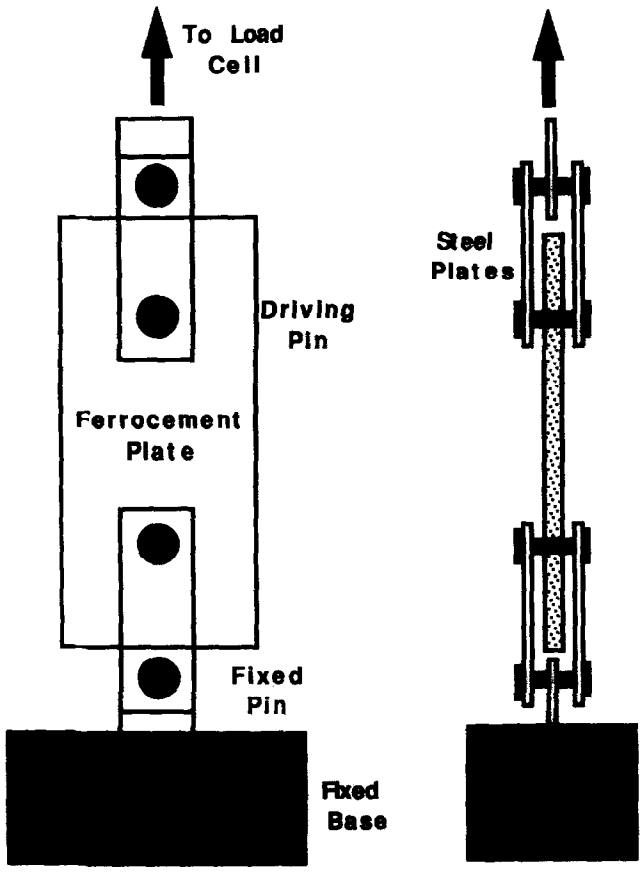

Fig. 2. Loading arrangement.

The data collection was carried out at a rate of 1 Hertz for all the specimens. The displacements were measured by both targets and LVDTs. The LVDTs were placed in proper fixtures attached to the specimens Seven targets and two LVDT's were utilized. The LVDT's were utilized to measure the displacements between the bolts and the displacements in the mid-portion region of the plate.

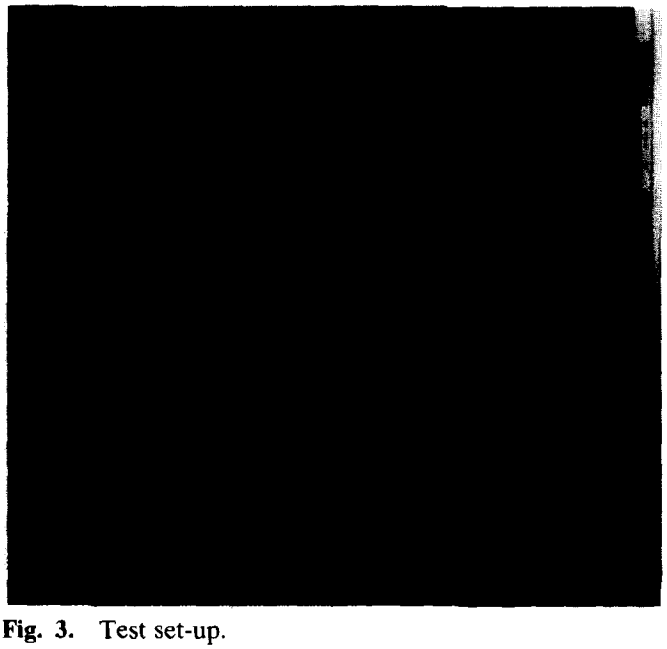

Fig. 3. Test set-up.

The control specimens were subjected to direct tensile loading. The end portion of the plates were placed in the grips of the testing machine, and the test was carried under displacement control. Displacements were measured by two LVDT's over a gage length of 7.9 in. (200.7 mm), as well as by an extensometer that measured the relative movement of the actuator head.

RESULTS AND DISCUSSION

Control specimens

The control specimens were primarily tested to obtain the strength of the reinforcing meshes as well as to get an idea of the tensile strength of the composite. The strength per layer per unit length was computed. This was obtained by dividing the total strength by the number of layers and by the width of the specimen. For the specimens reinforced with the square mesh in the 0/90° and in the $\pm 45°$ configuration, the average strength observed was 108 lbs/layer per in. (18.9 N/layer per mm). For the hexagonal mesh, the average values for the longitudinal and transversal directions were 45.3 lbs/layer per in. (7.9 N/layer per mm) and 31.6 lbs/layer per in. (5.5 N/layer per mm) respectively. For the hexagonal mesh, the strength in the longitudinal direction was 1.43 times the one in the transversal direction. The stress versus strain curves of the composite control specimens tested are shown in Fig. 4 and Fig. 5.

Failure modes

Among the pin-loaded ferrocement plates tested under tensile load, three failure modes were observed, cleavage failure, tensile failure and crushing bearing failure. The failure modes and the mesh configurations for which they occurred are summarized in Fig. 6.

The cleavage failure mode is characterized by a major crack, parallel to the plate longitudinal (or loading) direction, that extends from the hole to the plate edge. First, a small crack was initiated in the portion of the plate just ahead of the bolt and stopped at a small distance along a line parallel to the loading direction.

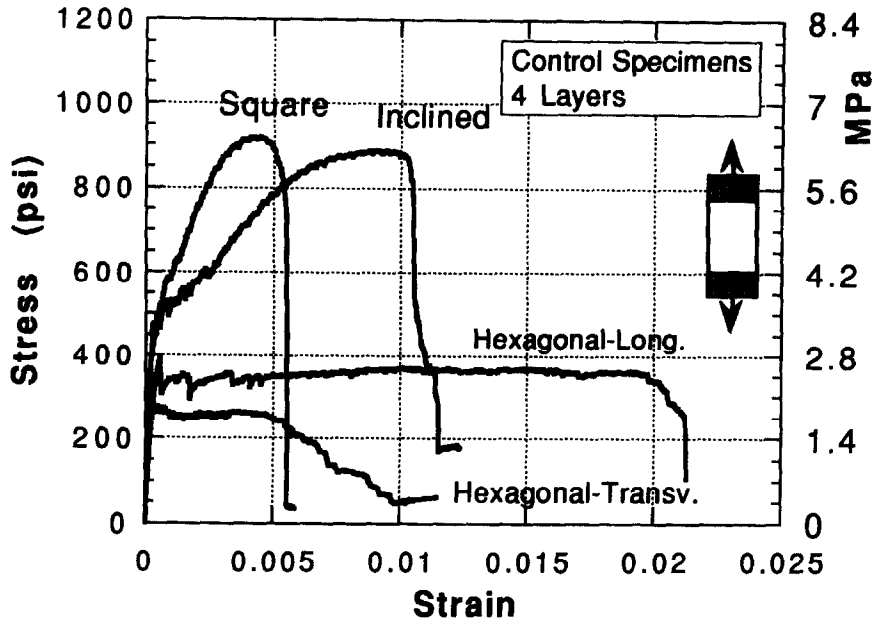

Fig. 4. Stress vs strain curves of control specimens, four mesh layers (1000 psi = 7 MPa).

Along the same line another crack was initiated at the edge of the plate. At a certain load level, the two cracks propagated to meet and formed one major crack that extended from the hole to the edge of the plate. As the load increased, the crack opened until the ultimate load was reached. A close inspection of the specimens that failed by cleavage showed that cracks were also initiated on the sides of the holes along the net tensile section. However, these cracks did not cause the final failure of the specimens.

In the tensile failure mode, a major crack emanates from the hole along the net-section, and propagates, normally to the loading direction, up to the lateral edges of the plate. While other cracks also develop during increased loading, the main tensile crack controls the final load-carrying capacity.

The crushing failure mode is characterized by the compressive crushing of the ferrocement material ahead of the hole due to the high bearing stresses caused by the contact between bolt

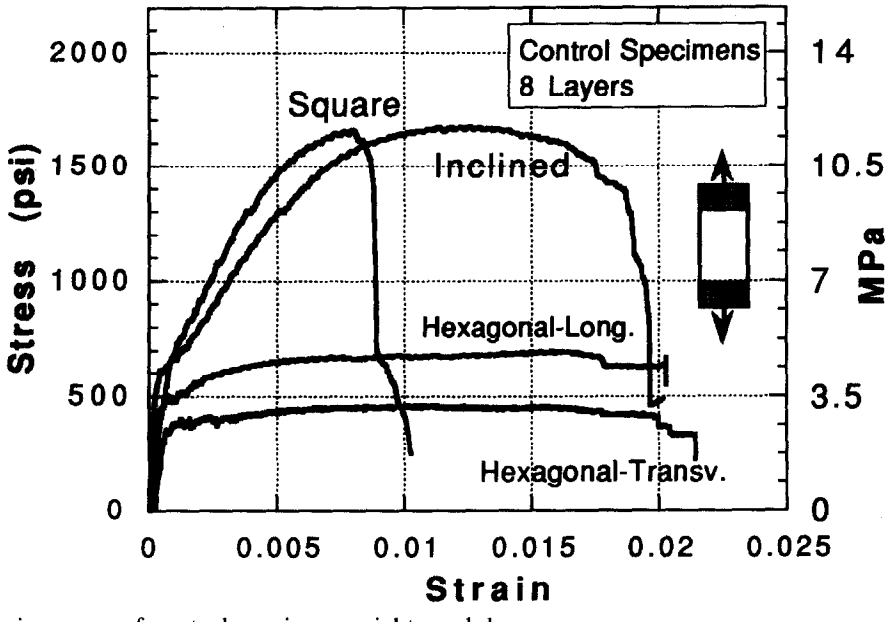

Fig. 5. Stress vs strain curves of control specimens, eight mesh layers.

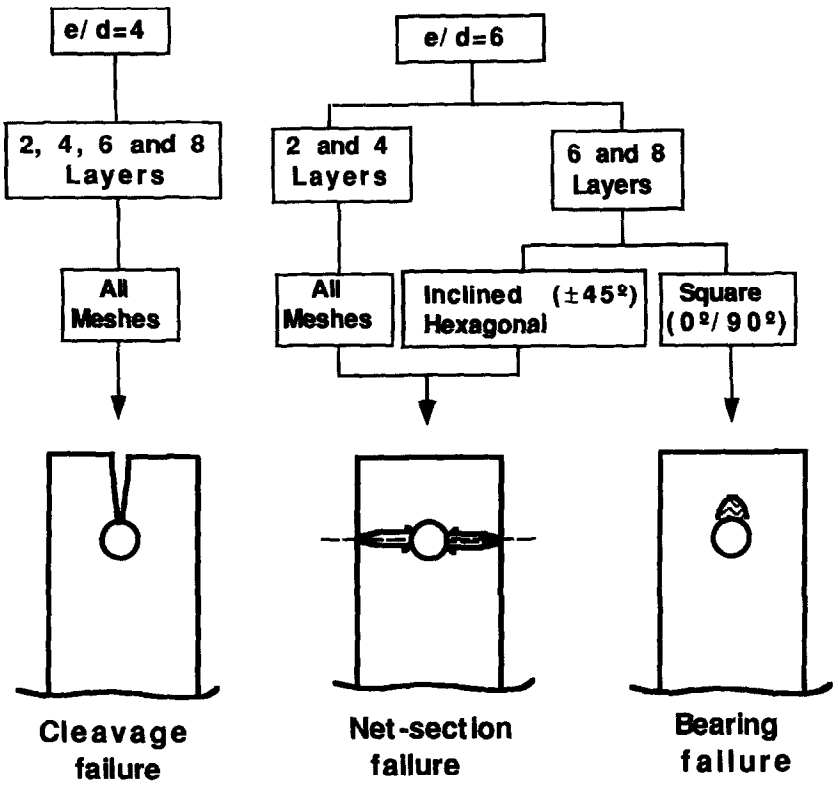

Fig. 6. Observed failure modes.

and hole. It is accompanied by spalling of the mortar in the vicinity of the hole; the hole diameter increases significantly.

Typical tested specimens reinforced with the square mesh at 0/90° are shown Fig. 7 where the three failure modes are clearly observed.

Effect of ratio *e/d*

The ratio of edge distance to bolt diameter (*e/d*) affected the failure mode of the specimens, and consequently the ultimate load capacity. For $e/d = 4$, all the specimens failed in the

Fig. 7. Photograph of specimens after failure: top four specimens: cleavage; bottom left (two): net-section tensile; bottom right (two): compression crushing.

cleavage failure mode. As the *e/d* was increased to 6, the failure mode was changed from one of cleavage to one of tensile net-section in all specimens reinforced in the inclined and hexagonal configurations, and in the specimens reinforced with two and four layers of mesh in the square configuration. The change in failure mode is illustrated in Fig. 8 for specimens reinforced with eight layers of the square inclined mesh. In this plot, a comparison is also made with a control specimen on the basis of composite stress.

In the specimens reinforced with six and eight layers of mesh in the square configuration (90°), a crack was initiated along the net-section, but the final failure was determined by crushing of the mortar ahead of the bolt.

Effect of number of mesh layers

In general, an increase in the number of mesh layers or volume fraction of reinforcement caused an increase in ultimate strength. However, the increase in strength was limited by the failure mode observed. The resistance per layer, obtained by dividing the failure load by the number of layers, gives an idea of the effectiveness of the different types of mesh used for each failure mode. These values were computed and summarized in Table 1. Note that for the specimens with $e/d = 6$ reinforced with the mesh in the square configuration, the increase in the number of mesh layers (up to eight layers) caused a change of failure mode from one of net-section tensile failure to one of crushing ahead of the bolt.

For the specimens reinforced in the square and inclined mesh configurations, where cleavage failure occurred, the contributions per layer of mesh to the overall resistance, were very similar. This suggests a strong correlation between the amount of reinforcement and the ultimate capacity of the plate. Because the displacement at maximum load also increases with the number of layers, the energy absorbed per layer increases with the number of layers (Figs 9 and 10). For the specimens reinforced in the hexagonal configuration, the contributions per layer differ significantly for the smaller volume fractions used, and it becomes more uniform as the number of layers increases. This suggests that for smaller amounts of reinforcement, the resistance of the mesh alone in the section where failure occurs is smaller than the cracking resistance of the section. Therefore, once the major cleavage crack reaches a critical size and propagates, the reinforcement cannot resist the load, causing a sudden load drop. The load versus bolt displacement response shows clearly the sudden load drop in the specimens reinforced with two and four layers, which confirms the hypothesis of sudden crack propagation (Fig. 11). However, if we analyze the post-cracking behavior of these two specimens, we

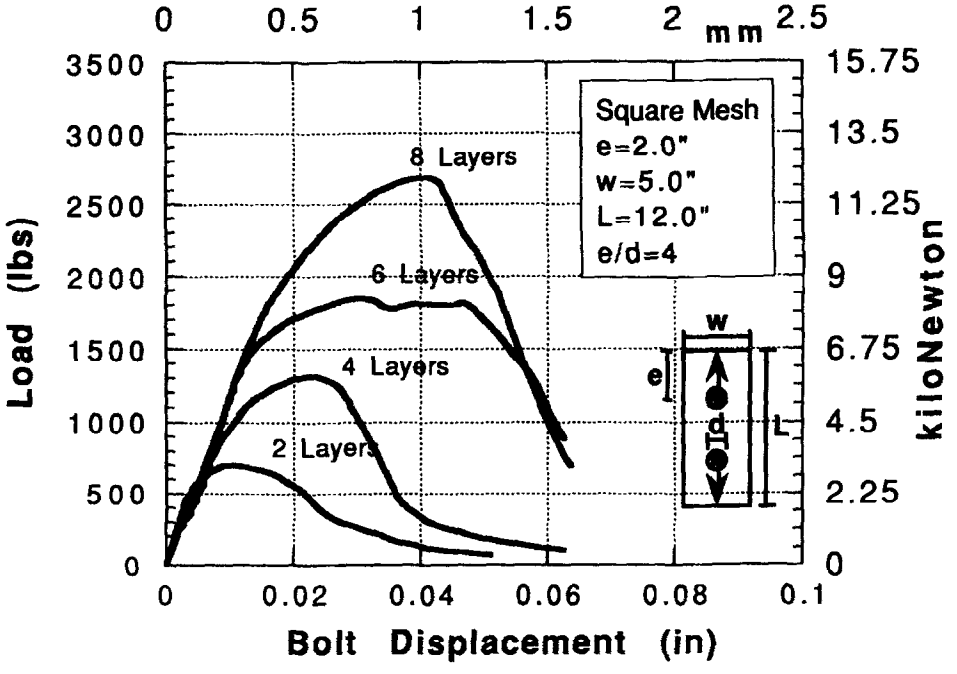

Fig. 8. Effect of e/d and comparison with control specimen; (1000 psi = 7 MPa).

Table 1. Summary of experimental results

Type of mesh	*Number of layers*	*Volume fraction (%)*	*e/d*	*Failure load Ptest lbs (N)*	*Failure mode*	*Strength/ layer lbs (N)*	*Resistance cleavage Rcl lbs (N)*	*Resistance tensile Rt lbs (N)*	*Ratio λ: resistance/ Ptest*
square	2	1.68	4	697 (3100.4)	cleavage	349 (1552.4)	378.0 (1681.4)	972.0 (4323.7)	λcl = 0.54
square	4	3.36	4	1297 (5769.3)	cleavage	324 (1441..2)	756.0 (3362.9)	1944.0 (8647.3)	λcl = 0.58
square	6	5.04	4	1894 (8424.9)	cleavage	316 (1405.6)	1134.0 (5044.3)	2916.0 (12971)	λcl = 0.60
square	8	6.72	4	2636 (11726)	cleavage	330 (1467.9)	1512.0 (6725.7)	3888.0 (17295)	λcl = 0.57
hexagonal	2	0.96	4	527 (2344.2)	cleavage	264 (1174.3)	158.5 (705.04)	284.4 (1265.1)	λcl = 0.3*
hexagonal	4	1.92	4	597 (2655.6)	cleavage	149 (662.8)	317.1 (1410.5)	568.8 (2530.1)	λcl = 0.53*
hexagonal	6	2.88	4	801 (3563.0)	cleavage	133 (591.6)	475.6 (2115.6)	853.2 (3795.2)	λcl = 0.59
hexagonal	8	3.84	4	993 (4417.1)	cleavage	124 (551.6)	634.2 (2821.1)	1137.6 (5060.3)	λcl = 0.64
inclined	2	1.68	4	559 (2486.6)	cleavage	279 (1241.1)	378.0 (1681.4)	972.0 (4323.7)	λcl = 0.68
inclined	4	3.36	4	1105 (4915.3)	cleavage	276 (1227..7)	756.0 (3362.9)	1944.0 (8647.3)	λcl = 0.68
inclined	6	5.04	4	1781 (7922.3)	cleavage	297 (1321.1)	1134.0 (5044.3)	2916.0 (12971)	λcl = 0.64
inclined	8	6.72	4	2402 (10685)	cleavage	300 (1334.5)	1512.0 (6725.7)	3888.0 (17295)	λcl = 0.63
mixed	4 squ., 2 hex.	4.32	4	1599 (7112.7)	cleavage	—	914.5 (4067.9)	2228.4 (9912.4)	λcl = 0.57
mixed	4 squ., 4 hex.	5.28	4	1770 (7873.4)	cleavage	—	1073.1 (4773.4)	2512.8 (11177)	λcl = 0.61
mixed	4 squ., 2 incl.	5.04	4	1837 (8171.4)	cleavage	—	1134.0 (5044.3)	2916.0 (12971)	λcl = 0.62
mixed	4 squ., 4 incl.	6.72	4	2252 (10017)	cleavage	—	1512.0 (6725.7)	3888.0 (17295)	λcl = 0.67
square	2	1.68	6	1057 (4701.8)	tensile	528 (2348.7)	594.0 (2642.2)	972.0 (4323.7)	λt = 0.92
square	4	3.36	6	2136 (9501.4)	tensile	534 (2375.4)	1188.0 (5284.5)	1944.0 (8647.3)	λt = 0.91
square	6	5.04	6	2736 (12170)	crushing	456 (2028.4)	1782.0 (7926.7)	2916.0 (12971)	—
square	8	6.72	6	2900 (12900)	crushing	362 (1610.3)	2376.0 (10569)	3888.0 (17295)	—
hexagonal	2	0.96	6	566 (2517.7)	tensile	283 (1258.8)	249.1 (1108.1)	284.4 (1265.1)	λt = 0.5*
hexagonal	4	1.92	6	639 (2842.4)	tensile	160 (711.7)	498.3 (2216.5)	568.8 (2530.1)	λt = 0.89*
hexagonal	6	2.88	6	816 (3629.7)	tensile	136 (605.0)	747.4 (3324.6)	853.2 (3795.2)	λt = 1.04
hexagonal	8	3.84	6	1074 (4777.4)	tensile	134 (596.1)	996.6 (4433.1)	1137.6 (5060.3)	λt = 1.06
inclined	2	1.68	6	877 (3901.1)	tensile	438 (1948.3)	594.0 (2642.2)	972.0 (4323.7)	λt = 1.1
inclined	4	3.36	6	1546 (6877.0)	tensile	386 (1717.0)	1188.0 (5284.5)	1944.0 (8647.3)	λt = 1.26
inclined	6	5.04	6	2687 (11952)	tensile	448 (1992.8)	1782.0 (7926.7)	2916.0 (12971)	λt = 1.08
inclined	8	6.72	6	3410 (15168)	tensile	426 (1894.9)	2376.0 (10569)	3888.017295)	lt = 1.14

*Ultimate load controlled by the cracking load.

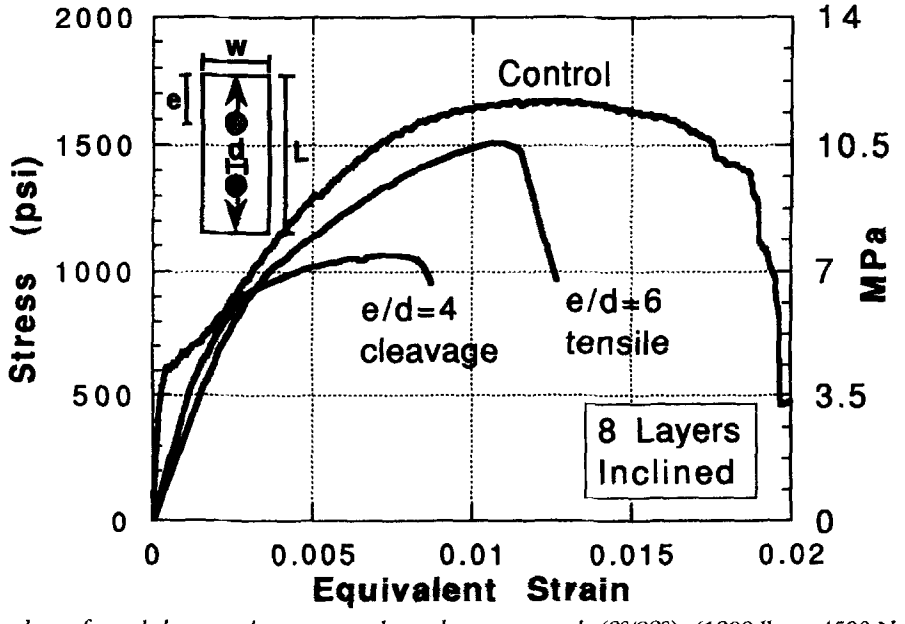

Fig. 9. Effect of number of mesh layers, cleavage mode and square mesh (0°/90°); (1000 lbs = 4500 N; 1 in. = 25 mm).

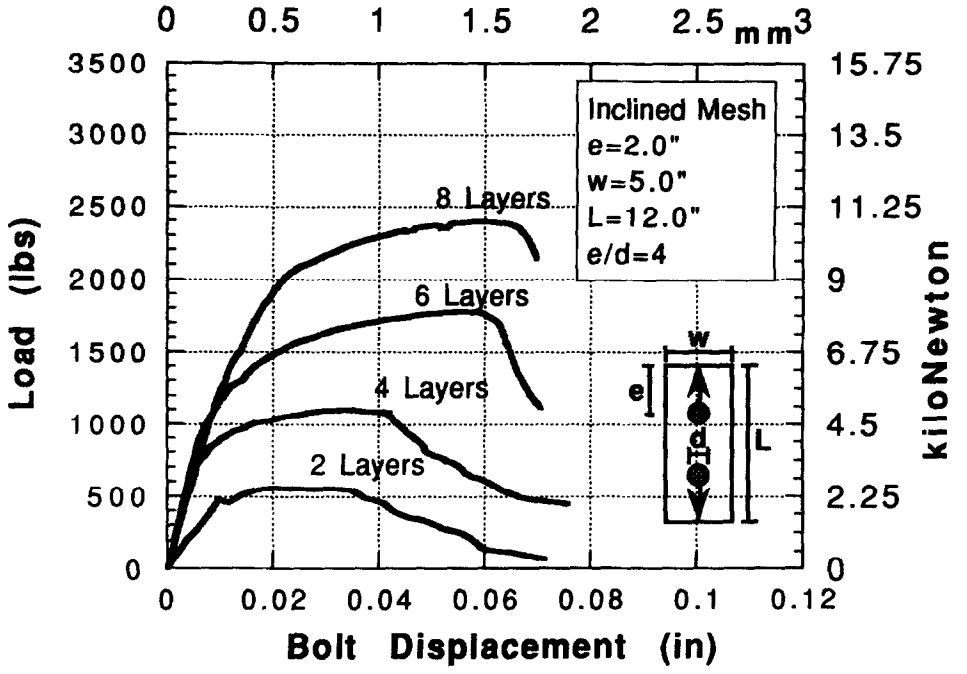

Fig. 10. Effect of number of mesh layers, cleavage mode and inclined mesh ($\pm 45°$); (1000 lbs = 4500 N; 1 in. = 25 mm).

observe a load plateau of 125 lbs/layer (556.0 N/layer) and 112.5 lbs/layer (500.1 N/layer) for the specimens reinforced with two and four layers, respectively; these values are similar to the ones obtained for specimens reinforced with higher volume fractions. The specimens where a combination of meshes was used, also failed in the cleavage failure mode, and the addition of mesh layers increased the load capacity (Fig. 12).

The specimens reinforced in the square and inclined configurations that failed by tension along the net-section showed very similar values of contribution per layer to the total resistance. The load versus bolt displacement response of specimens reinforced with the inclined mesh, points clearly to the strength dependency on the amount of reinforcement (Fig. 13). However, in the specimens reinforced in the hexagonal con-

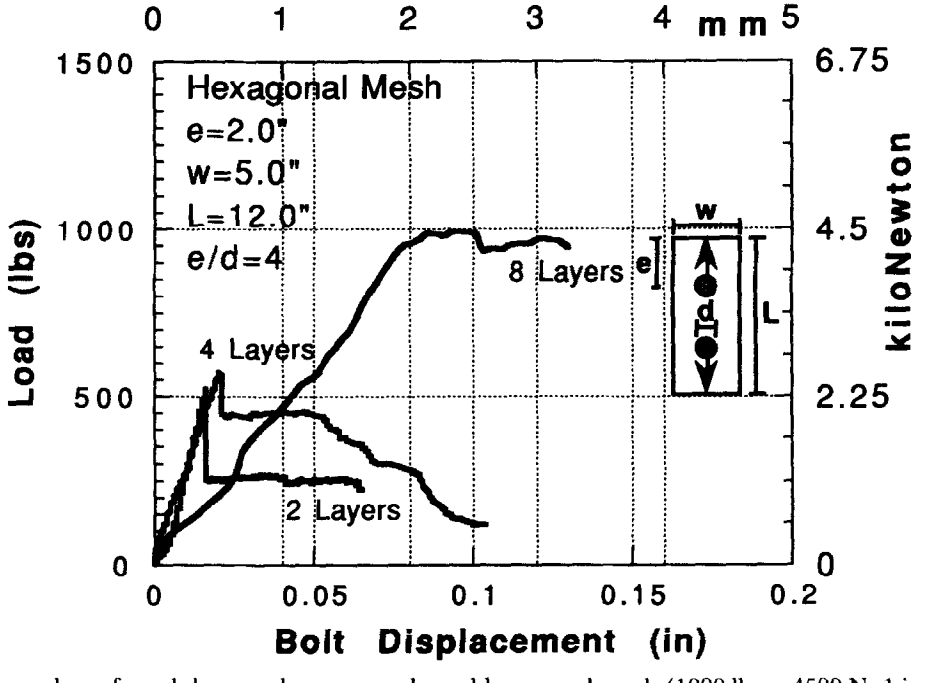

Fig. 11. Effect of number of mesh layers, cleavage mode and hexagonal mesh (1000 lbs = 4500 N; 1 in. = 25 mm).

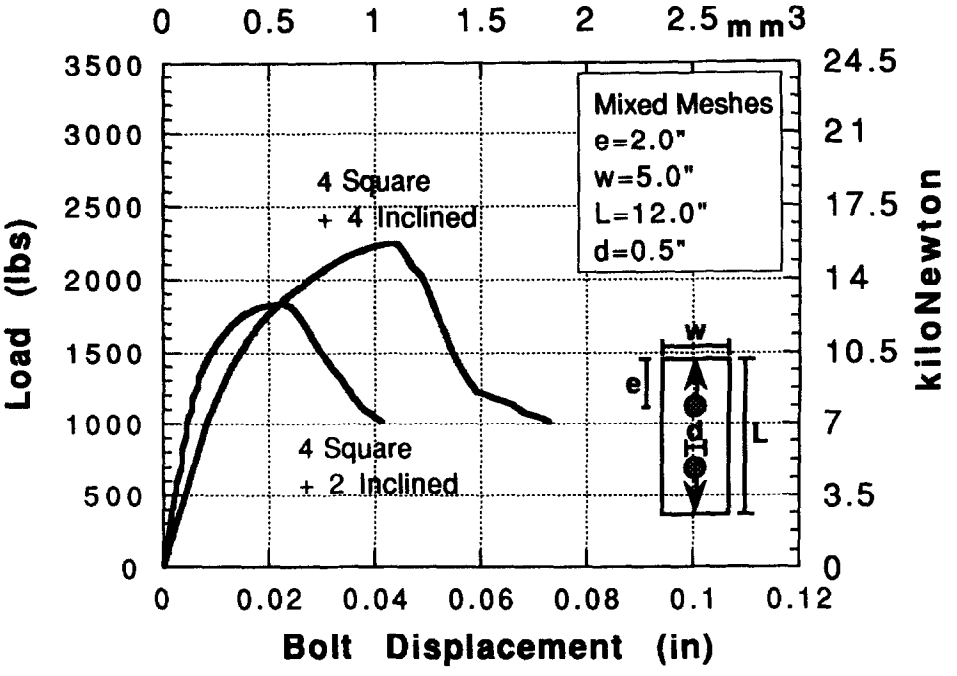

Fig. 12. Effect of number of mesh layers, cleavage mode and mixed mesh (1000 lbs = 4500 N; 1 in. = 25 mm).

figuration, the resistance per layer in avoiding the net-section failure is higher for the smaller volume fractions used, and tends to a value of approximately 135 lbs/layer (600.5 N/layer) as the number of layers increases. We can explain this by the same argument utilized earlier, that is for the small number of layers, the resistance of the mesh alone along the net section is smaller than the composites' cracking resistance (Fig. 14).

In the specimens that failed by crushing, the contribution per layer decreases with an increase in the number of layers, suggesting that after a certain limit, the reinforcement is somewhat inefficient in resisting the crushing failure mode (Fig. 15).

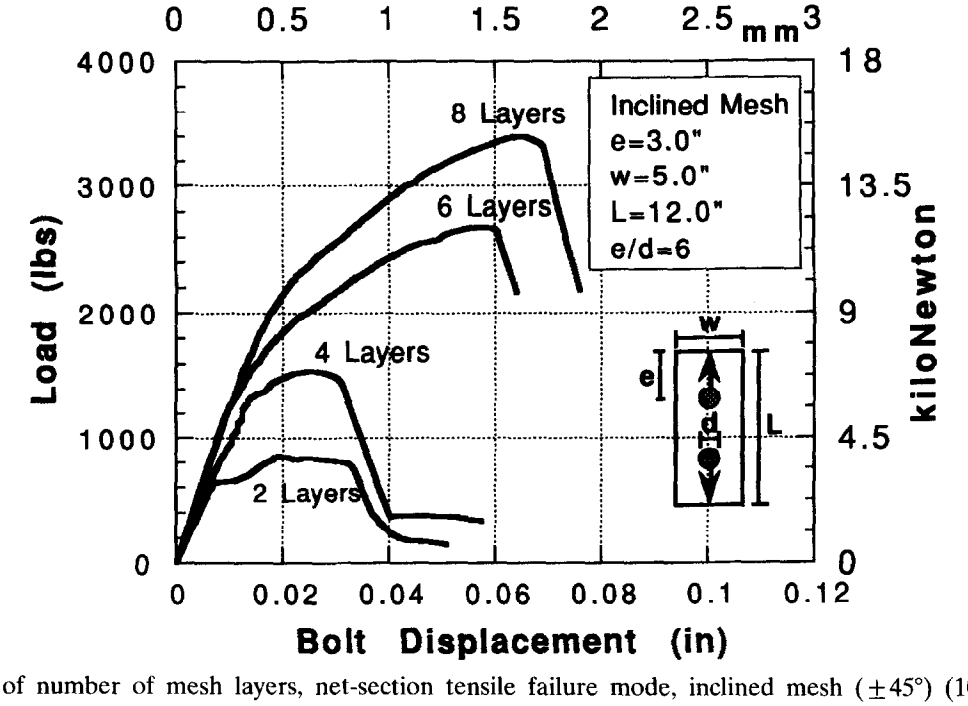

Fig. 13. Effect of number of mesh layers, net-section tensile failure mode, inclined mesh (±45°) (1000 lbs = 4500 N; 1 in. = 25 mm).

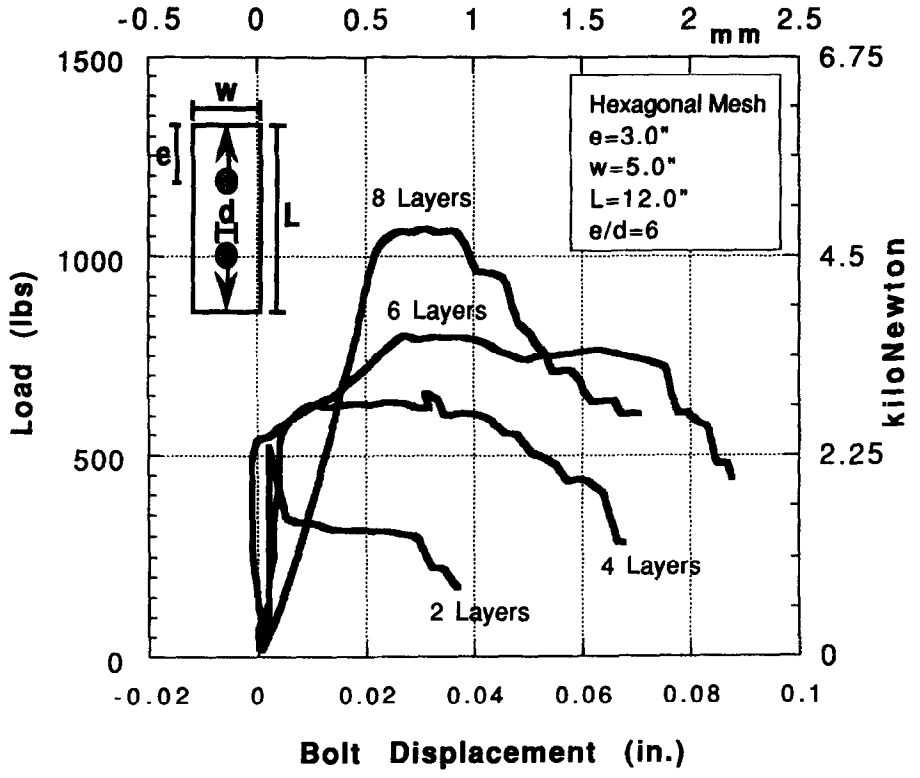

Fig. 14. Effect of number of mesh layers, net-section tensile failure mode and hexagonal mesh (1000 lbs = 4500 N; 1 in. = 25 mm).

Effect of type of mesh and mesh orientation

In order to find the effectiveness of each mesh, a comparison between different meshes is made on the basis of the load capacity for a certain amount of reinforcement. The comparison between specimens reinforced with the square and inclined layers of mesh can be made directly on the basis of the number of layers, since the total volume fraction of reinforcement is identical. However, the amount of reinforcement per unit area of the square mesh is 1.75

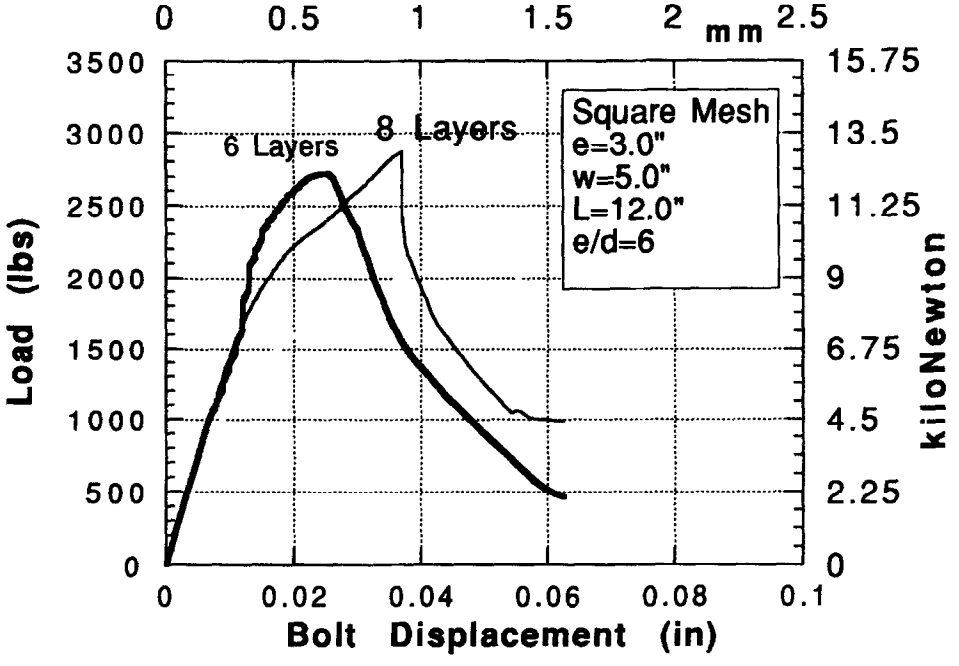

Fig. 15. Effect of number of mesh layers, crushing mode and square mesh (0°/90°) (1000 lbs = 4500 N; 1 in. = 25 mm).

times that of the hexagonal mesh. Therefore, this factor was utilized to compare the performance of the two meshes.

For the specimens that underwent the cleavage failure mode, the square mesh was the most effective mesh, followed by the inclined and hexagonal meshes, respectively (Fig. 16). The average strength ratio between the specimens reinforced with the square mesh and the inclined mesh was 1.14, implying that little loss in strength is observed when loading at an angle. When comparing square with hexagonal meshes on the basis of total amount of reinforcement, and excluding the specimens where the cracking determined the ultimate load (two and four layers of the hexagonal mesh), an average strength ratio of 1.43 is observed in favor of the square mesh. The 'mixed' specimens where a combination of mesh types were used, had a performance that was comparable and could be predicted using an averaging procedure.

For the specimens that had the net-section tensile failure mode, the square mesh was the most effective, followed by the inclined and hexagonal meshes, respectively. The average strength ratio for specimens reinforced with the square and inclined meshes, was 1.27. The ratio was 1.88 for specimens reinforced with the four layers of square and hexagonal meshes.

The crushing failure mode did not occur in the specimens reinforced with the inclined mesh, even for the highest number of layers, leading therefore to a better performance of the inclined mesh relative to the square mesh (Fig. 17).

LIMIT ANALYSIS AND PREDICTION EQUATIONS

To derive prediction equations, the lower bound theorem of limit analysis was used. The theorem states that if an equilibrium distribution of stresses, that are everywhere below yield, is found, then collapse will not occur. To utilize this theorem and obtain lower bounds for the strength of ferrocement shear connections, the known components of the external loads must be related to the resistance along the various sections.

An extensive finite element analysis was undertaken to find the stress distribution along the critical sections; detailed results are presented in refs 7 and 12. A schematic representation of these stresses is shown in Fig. 18. The applied force P is transmitted to the plate through the pressure distribution ahead of the bolt; it can be substituted by two equivalent loads, one parallel to the longitudinal direction of the plate $P_{y/2}$, and one parallel to the transversal direction of the plate P_x (Fig. 19). At ultimate, these load components have to be resisted by the various sections along the plate.

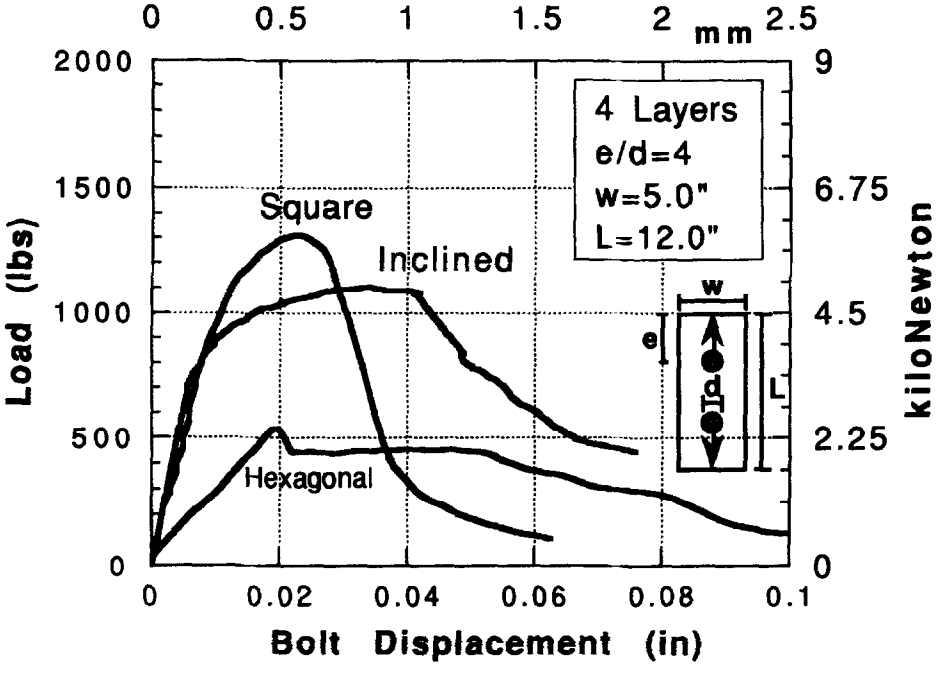

Fig. 16. Effect of mesh type/orientation, e/d = 4 (1000 lbs = 4500 N; 1 in. = 25 mm).

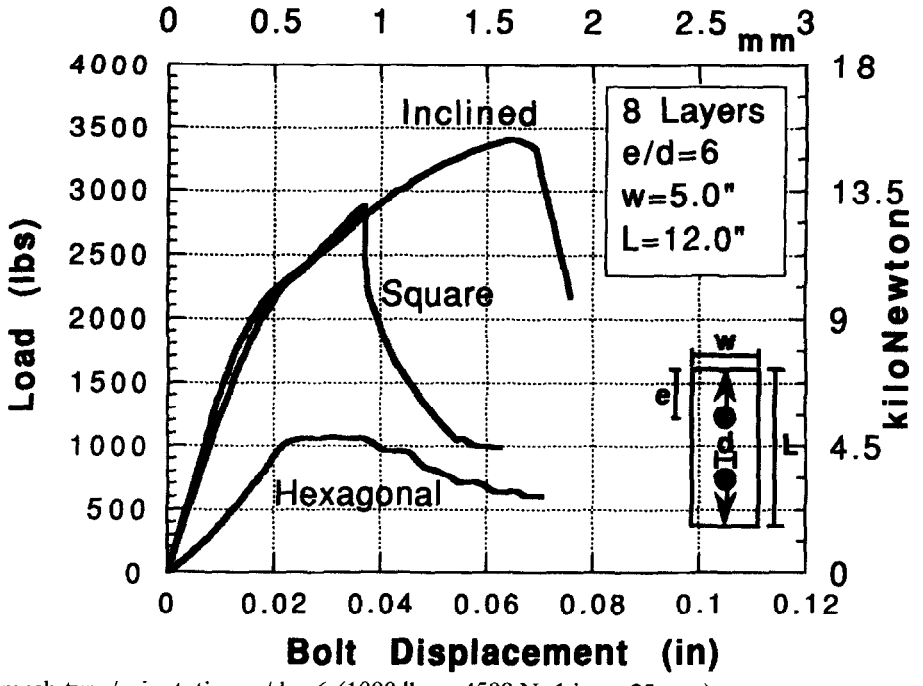

Fig. 17. Effect of mesh type/orientation, e/d = 6 (1000 lbs = 4500 N; 1 in. = 25 mm).

Failure will occur when the applied external loads induce stresses that exceed the ultimate resistance along one of the critical sections. In order to avoid the bearing type of failure, the bearing stresses induced around the hole also have to be resisted by the material near the hole boundary.

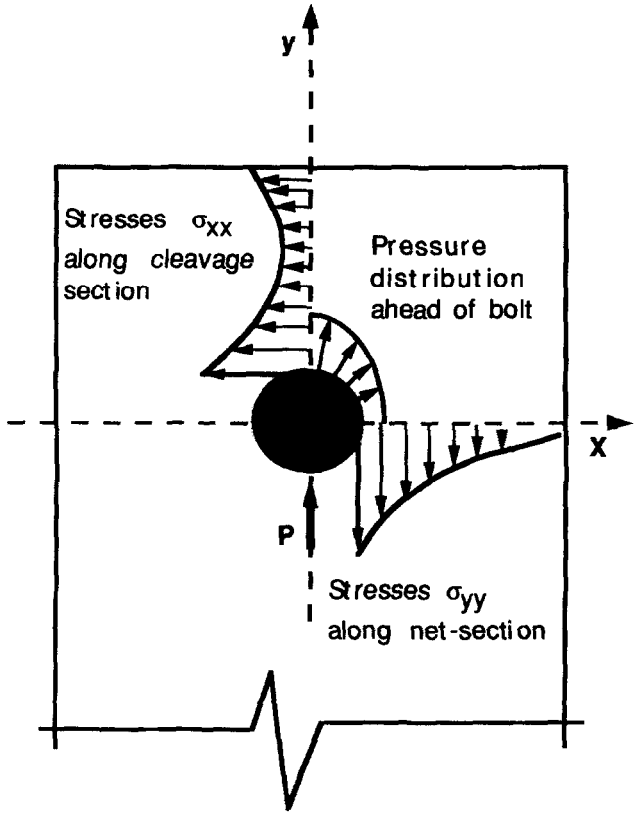

Fig. 18. Critical sections and corresponding stress distribution.

Cleavage failure

In the cleavage failure mode, crack propagation is followed by crack widening, which in turn is accompanied by plastic flow of the reinforcing meshes that cross the crack. A cleavage type of failure will occur when the steel mesh system yields along the entire cracked section. This behavior was observed experimentally and was also confirmed in the finite element analysis.

From equilibrium, the ultimate resistance obtained (assuming yielding of the reinforcing meshes that cross the cleavage section) must be equal to the applied external load P_x in the x-direction. However, P_x can only be computed by integration, along the hole boundary, of the horizontal components of the pressure, which are obtained from a finite element analysis. In the non-linear FE analysis undertaken[12], it was observed that the ratio P_x/P_y, where P_y is the applied load, reaches a value exceeding 0.53 before collapse, and the ratio was increasing with P_y.

In this study, a coefficient λ_{cl} representing the ratio of ultimate resistance along the cleavage section (to resist P_x) to the applied load P_y was defined. The value of P_x was obtained assuming yielding of the reinforcement along the cleavage section; the value of P_y was taken as the failure

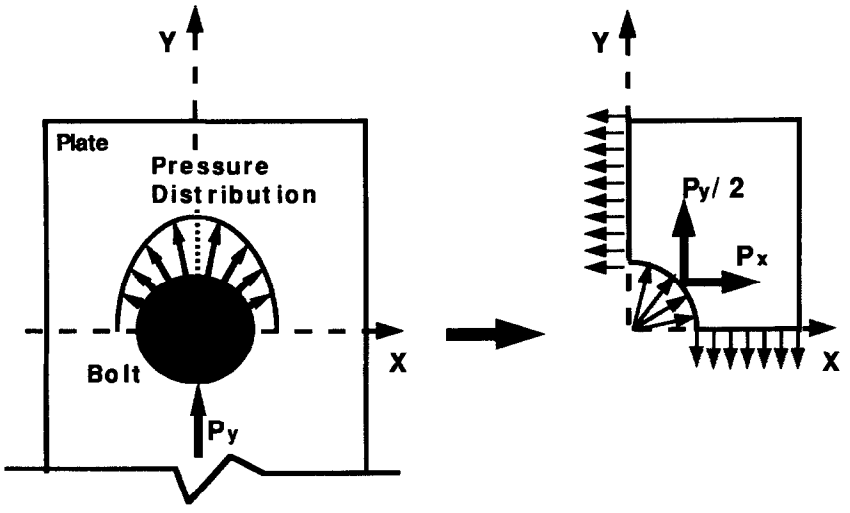

Fig. 19. Equivalent system of forces acting on plate.

load. The values of λ_{cl} obtained for the specimens that underwent a cleavage failure mode are presented in Table 1. It can be observed that they vary between 0.54 and 0.66 (excluding the two specimens reinforced with two and four layers of hexagonal mesh, since their failure was dictated by the cracking strength). Their average values were 0.57, 0.61, 0.66 and 0.62 for the square, hexagonal, inclined and mixed configurations, respectively.

For design, an average value of $\lambda_{cl} = 0.6$ is recommended here, leading to the following prediction equation of ultimate capacity of the connection before cleavage failure occurs:

$$P_{cl} = N(e - d/2)R_{cl}/0.6 \qquad (1)$$

where P_{cl} is the component of external force applied in the bolt hole parallel to the longitudinal direction of the plate that causes cleavage failure, N is number of layers of reinforcing mesh, e is distance between the center of the hole and the plate edge, d is the hole diameter, R_{cl} is the yield resistance per unit width of one layer of reinforcing mesh crossing the cleavage section (lbs/inch per layer). If different meshes are used, the resistances per layer are additives.

Predicted values using eqn (1) show good agreement with the experimental results (Table 2). For the specimens where true cleavage failure occurred, the ratio of predicted to experimental ultimate load has a mean almost equal to 1. Note that for small volume fractions

Table 2. Comparison between prediction formulae and test results for the cleavage failure mode

Type of mesh	*Number of layers*	*Volume fraction (%)*	*e/d*	*Failure load Ptest lbs (N)*	*Pcl = (N(e−d/2) R_{lc})/0.6) lbs (N)*	*Pcl/Ptest*	*Psh = (e h (ft fc*)$^{1/2}$)^{11} lbs (N)*	*Psh/Ptest*
square	2	1.68	4	697 (3100.4)	624 (2775.7)	0.89	1388 (6174.1)	2.00
square	4	3.36	4	1297 (5769.3)	1248 (5551.4)	0.96	1964 (8736.3)	1.51
square	6	5.04	4	1894 (8424.9)	1872 (8327.1)	0.99	2405 (10698)	1.26
square	8	6.72	4	2636 (11726)	2497 (11107)	0.95	2777 (12353)	1.05
hexagonal	2	0.96	4	527 (2344.2)	264 (1174.3)	0.50*	903 (4016.7)	1.72
hexagonal	4	1.92	4	597 (2655.6)	528 (2348.7)	0.88*	1278 (5684.8)	2.13
hexagonal	6	2.88	4	801 (3563.0)	792 (3523.0)	0.99	1565 (6961.5)	1.96
hexagonal	8	3.84	4	993 (4417.1)	1057 (4701.8)	1.06	1807 (8037.9)	1.82
inclined	2	1.68	4	559 (2486.6)	624 (2775.7)	1.12	1388 (6174.1)	2.5
inclined	4	3.36	4	1105 (4915.3)	1248 (5551.4)	1.13	1964 (8736.3)	1.78
inclined	6	5.04	4	1781 (7922.3)	1872 (8327.1)	1.05	2405 (10698)	1.35
inclined	8	6.72	4	2402 (10685)	2497 (11107)	1.04	2777 (12353)	1.16
mixed	4 squ., 2 hex.	4.32	4	1599 (7112.7)	1512 (6725.7)	1.06	2162 (9617.1)	1.35
mixed	4 squ., 4 hex.	5.28	4	1770 (7873.4)	1776 (7900.0)	0.99	2343 (10422)	1.33
mixed	4 squ., 2 incl.	5.04	4	1837 (8171.4)	1872 (8327.1)	0.98	2405 (10698)	1.32
mixed	4 squ., 4 incl.	6.72	4	2252 (10017)	2496 (11103)	0.9	2777 (12353)	1.23

*Ultimate Load governed by the cracking load.

of reinforcement, the ultimate capacity of the cleavage section is determined by the fracture characteristics of the plate. In this case, eqn (1) will give conservative results, since the cracking load is higher than the load given by yielding of the reinforcement.

Net section failure

In the net-section tensile failure mode, a crack starts at the hole, where very high stress concentrations are present, and propagates gradually until it reaches the side end of the plate. Crack propagation is followed by crack widening, which in turn is accompanied by yielding of the reinforcing meshes that cross the crack. The ultimate load is reached when the steel mesh has yielded along the entire cracked section. The average ratio λ_t between the resistance of the net-section and the failure load for all specimens that presented this failure mode was approximately 1 (Table 1, last 12 specimens). Therefore, the following equation is recommended for design:

$$P_t = N(w-d)R_{\ln} \tag{2}$$

where P_t is the component of external force applied in the hole boundary, which is parallel to the longitudinal direction of the plate and causes the tensile failure mode, N is the number of layers of mesh, w is the width of the plate, d is the hole diameter, $R_{\ln}$ is the resistance (assuming yielding) per unit width of one layer of reinforcing mesh crossing the net-section (lbs/inch per layer). If different meshes are used, their resistances per layer can be added.

Compression bearing failure

This failure mode is related to the capacity of the ferrocement material in transferring the high compressive stresses near the hole. Only two specimens failed in the compression bearing mode. These specimens were reinforced with six and eight layers of the square mesh in the 0/90° (square) configuration. A lower bound prediction for this failure mode can be obtained by assuming a constant pressure distribution around the perimeter of the hole, equal to the compressive strength f'_c of the mortar. The contribution of the reinforcing mesh is neglected. The following prediction equation can then be derived for the ultimate load:

$$P_{cr} = f'_c dt \tag{3}$$

where P_{cr} (crushing load) is the resistance of the mortar material along the hole perimeter, f'_c is the compressive strength of the mortar, d is the hole diameter, and t is the thickness of the plate Values of P_{cr} predicted from eqn (3) were checked against experimental results. The ratio between the computed and actual failure loads were 0.77 and 0.73, for the specimens reinforced with six layers and eight layers of the square mesh in the 0/90° configuration, respectively. eqn (3) was also used to predict the strength of the two specimens that presented the crushing (bearing) failure mode, namely V_3 and V_4, reported by Mansur *et al.*[11] The ratio between the computed and actual failure loads was 0.87 and 0.86, respectively. It can be concluded that eqn (3) is conservative and can be used as a first approximation in design.

It is important to point out that, since bearing or crushing failure was not observed when the reinforcement was inclined at $\pm 45°$, eqn (3) is only applicable for specimens reinforced in the 0/90° configuration. Additional analysis and testing are needed to incorporate other cases.

COMPARISON WITH OTHER PREDICTION EQUATIONS

Some equations to predict the resistance of ferrocement connections were developed by Mansur *et al.*[11] They basically gave two equations, one to predict the strength in the tensile failure mode (P_t), and one in the shear failure mode (P_{sh}), as follows:

$$P_t = h(W-d)f_t \tag{4}$$

(from Mansur *et al.*[11])

$$P_{sh} = eh(f_t f_c^*)^{1/2} \tag{5}$$

(from Mansur *et al.*[11]) where h is the thickness of the ferrocement plate, W the width of the ferrocement plate, d the diameter of the bolt hole, f_t the tensile strength of ferrocement, e the edge distance of the bolt hole, and $f_c^* = v\, f'_c$ ($v = 0.53$ and f'_c the cylinder compressive strength of mortar). It can be observed that the tensile failure mode prediction formula is equivalent to the one presented in the current study (eqn (2)), except that it is written in terms of unit-area instead of unit-width strength. It is thus expected to yield similar numerical results.

The shear failure mode equation (eqn (5)) was used by Mansur *et al.*[11] to predict the shear, shear-cleavage, and cleavage failure modes with very good correlation with the experimental results presented in their investigation. In order to check the accuracy of eqn (5) with the experimental results of this study, the predicted resistance from eqn (5) was compared with the experimentally observed strength for the specimens that failed by cleavage. The results are summarized in Table 2. It can be observed that the ratios between the ultimate load values computed from eqn (5) and the test results of the current investigation (P_{sh}/P) vary between 1.16 and 2.5, implying a very poor correlation in most cases. This is possibly due to the fact that eqn (5) overestimates the contribution of the cement mortar in a pure cleavage failure mode. Based on these results, eqn (5) is not recommended for design; further evaluation is needed to ascertain the range of applicability of eqn (1) or eqn (5).

CONCLUSIONS

Based on the tests undertaken in this study and the range of parameters evaluated, the following conclusions can be drawn for bolted ferrocement joints.

(1) Three types of failure were observed in the pin-loaded ferrocement plates tested: namely, a cleavage failure ahead of the bolt, a tensile failure along the net-section width, and crushing of the ferrocement plate in the vicinity of the hole.
(2) Increasing the amount of mesh reinforcement is very effective in enhancing the resistance against the cleavage and net-section failure modes, while, at the boundary, it may lead to a crushing failure mode.
(3) For specimens where the cleavage failure occurred and on the basis of total amount of reinforcement, the square mesh in the 0/90° configuration was the most effective, followed by the square mesh in the $\pm 45°$ direction, then the hexagonal mesh.
(4) For ratios between the cleavage resisting section and the net-section less than about 0.39, a primarily cleavage failure mode occurs for pin-loaded ferrocement plates reinforced with the square mesh in the 0/90° direction, the square mesh in the $\pm 45°$ configuration, and the hexagonal mesh.
(5) For ratios between the cleavage resisting section and the net-section higher than about 0.61, tensile failure of the net section is predominant.
(6) When the volume fraction of square reinforcing mesh exceeded about 3.36%, a primarily compression failure occurred in the 0/90° reinforcing configuration.
(7) The prediction equations developed in this study to predict the loads leading to failure either by cleavage, or net-section tensile, or crushing compression, were in very good agreement with experimental results. They are recommended for use as a first approximation in design. It is noted, however, that for the crushing failure mode, which occurs only at high volume fractions of reinforcement, the proposed prediction equation is conservative. Thus failure occurs as soon as the applied external load, P, exceeds either one of the three load limits leading to one of the failure modes. Thus for design:

$$P \leq N(e - d/2)R_{cl}/0.6$$

$$P \leq N(w - d)R_{\ln}$$

$$P \leq f'_c dt$$

where N is number of layers of reinforcing mesh, e is distance between the center of the hole and the plate edge, d is the hole diameter, R_{cl} is the yield resistance per unit width of one layer of reinforcing mesh crossing the cleavage section (lbs/inch per layer), w is the width of the plate, $R_{\ln}$ is the resistance (assuming yielding) per unit width of one layer of reinforcing mesh crossing the net-section (lbs/inch per layer), f'_c is the compressive strength of the mortar, and t is the thickness of the plate.

ACKNOWLEDGEMENTS

This research was supported in part by a grant from the National Science Foundation to the NSF Center for Advanced Cement Based

Materials. Any opinions, findings and conclusions expressed in this study are those of the authors and not necessarily reflect the views of NSF or the ACBM center.

REFERENCES

1. Agarwal, B. L., Static strength prediction of bolted joints in composite materials. *AIAA Journal*, **18** 11 (1980) 1371–1375.
2. Agarwal, B. D. & Broutman, L. J., *Analysis and Performance of Fiber Composites*, John Wiley and Sons, New York, 1980.
3. Blake, A., *Design of Mechanical Joints*, Dekker, New York, 1985.
4. Chang, F., Scott, R. A. & Springer, G. S., Failure of composite laminates containing pin loaded holes — method of solution. *Journal of Composite Materials*, **18** (1984) 255–278.
5. Eriksson, L. I., Contact stresses in bolted joints of composite laminates. *Composite Structures*, **6** (1986) 57–75.
6. Krishnamoorthy, T. S., Parameswaran, V. S., Neelamegam, M. & Balasubramaniam, K., Investigation of precast ferrocement planks connected by steel bolts, *ACI Special Publication*, SP-124, 389–403.
7. Hammoud, H. Study of Ferrocement Bolted Connections for Structural Applications. Thesis submitted in partial fulfillment of a Ph.D., The University of Michigan, Ann Arbor, January 1993.
8. Naaman, A. E., Ferrocement housing: Toward integrated high technology solutions. *Journal of Ferrocement*, **19** 2 (1989) 141–149.
9. Naaman, A. E. & Hammoud, H., Ferrocement prefabricated housing: The next generation. *Journal of Ferrocement*, **22** 1 (1992) 35–47.
10. Hammoud, H. & Naaman, A. E., Behavior of Ferrocement Moment Resisting Joints, Presented at ACI Fall Convention, Puerto Rico, October, 1992, and *ACI Special Publication*, SP-146, pp. 111–130.
11. Mansur, M. A., Abdullah, & Alwis, W. A. M., Strength of bolted joints in ferrocement. *ACI Structural Journal*, **91** 3 (1994) 315–323.
12. Hammoud, H. & Naaman, A. E., Ferrocement bolted shear joints: Finite element analysis and stress distribution, Submitted for publication, proceedings of Sixth International Symposium on Ferrocement — Ferro 6, June 1998.